AIP | Applied Physics Letters

Formation of nanoscale magnetic bubbles in ferromagnetic insulating manganite La7/8Sr1/8MnO3

T. Nagai, M. Nagao, K. Kurashima, T. Asaka, W. Zhang, and K. Kimoto

Citation: Applied Physics Letters **101**, 162401 (2012); doi: 10.1063/1.4760266
View online: http://dx.doi.org/10.1063/1.4760266
View Table of Contents: http://scitation.aip.org/content/aip/journal/apl/101/16?ver=pdfcov
Published by the AIP Publishing

Formation of nanoscale magnetic bubbles in ferromagnetic insulating manganite $La_{7/8}Sr_{1/8}MnO_3$

T. Nagai,[1] M. Nagao,[1] K. Kurashima,[1] T. Asaka,[2] W. Zhang,[1] and K. Kimoto[1]
[1]*Transmission Electron Microscopy Station and Surface Physics and Structure Unit, National Institute for Materials Science (NIMS), Tsukuba 305-0044, Japan*
[2]*Department of Materials Science and Engineering, Nagoya Institute of Technology, Nagoya 466-8555, Japan*

(Received 16 July 2012; accepted 3 October 2012; published online 15 October 2012)

We have observed the response of spin arrangements to external magnetic fields in a multiorbital Mott insulator, ferromagnetic insulating manganite $La_{7/8}Sr_{1/8}MnO_3$, by low-temperature *in situ* Lorentz microscopy. Magnetic fields normal to the plane of the thin-plate sample continuously change the width of domains in the serpentine-like domain structure, eventually giving rise to nanoscale elliptical magnetic bubbles of ~200 nm major diameter at 3.6 kOe. The formation of these bubbles implies large magnetic anisotropy related to the orbital ordering and suggests the possibility of manipulating the bubbles using an electric field. © *2012 American Institute of Physics*. [http://dx.doi.org/10.1063/1.4760266]

Nanoscale magnetic patterns currently play a key role in spintronics. In particular, the manipulation of these patterns using an applied electric field is an important issue.[1] Magnetic bubbles are potential magnetic bits in nonvolatile and high-density recording memories;[2–4] serpentine-like domains are transformed into bubble domains by an external magnetic field normal to the sample plane in the thin plates of some magnets. Although the manipulation of these bubbles using an electric field has not yet been realized, a theoretical study has recently shown the possibility of their manipulation in ferromagnetic (FM) multiorbital Mott insulators where an interaction between the electric field and spins occurs.[5,6] However, large uniaxial magnetic anisotropy (K_u) is required to produce the bubbles; therefore, few types of magnets exhibiting spontaneous magnetization, such as spin-canted orthoferrites RFeO$_3$ (R: rare-earth element) and ferrimagnetic iron-garnets R_3(Fe, M)$_5$O$_{12}$ (M: Al, Ga, In), have been reported to produce them. To our knowledge, magnetic bubbles have seldom been observed for ferromagnets [Fig. 1(a)] and, further, have not been observed for FM multiorbital Mott insulators.

On the other hand, perovskite manganites (R,A)MnO$_3$ (A: alkaline earth element), which are typical of strongly correlated multiorbital electron systems, have attracted considerable attention owing to their unusual magnetic and electronic properties such as colossal magnetoresistance (CMR). Undoped LaMnO$_3$ is an antiferromagnetic (AFM) orbital-ordered (OO) Mott insulator with a cooperative Jahn-Teller distortion ($T_{OO} = 780$ K, $T_N = 140$ K).[7] Doped La$_{1-x}$Sr$_x$MnO$_3$ (LSMO) exhibits various electronic phases: it is a spin-canted AFM insulator ($T < T_N$) or a paramagnetic (PM) insulator ($T \geq T_N$) when $0 < x < 0.1$; a FM insulator ($T < T_{MI}$), a FM metal ($T_{MI} \leq x < T_C$) or a PM insulator ($T \geq T_C$) when $0.1 \leq x \leq 0.15$; a FM metal ($T < T_C$) or a PM insulator ($T \geq T_C$) when $0.15 < x < 0.3$; and a FM metal ($T < T_C$) or a PM metal ($T \geq T_C$) when $0.3 \leq x \leq 0.6$.[8] Since the double exchange mechanism fails to explain the coexistence of ferromagnetism and insulating behavior, the FM insulating phase has attracted considerable attention.[9–13] Furthermore, recent studies indicate that orbital ordering is critical for this phase to appear[14] and that this FM phase is one of the multiorbital Mott insulators, which include BiMnO$_3$, La$_2$NiMnO$_6$, and La$_2$CoMnO$_6$.[5,15]

In this letter, we report the direct observation of nanoscale magnetic bubbles in a multiorbital Mott insulator, i.e., the OO FM insulating phase of the lightly doped perovskite manganite LSMO at $x = 1/8$, by low-temperature *in situ* Lorentz microscopy (LM). Our study suggests the possibility of manipulating nanoscale bubbles forming in a FM insulator using an electric field. The LM method is one of the most advanced magnetic imaging techniques for visualizing magnetic structures at a high spatial resolution.[16] In the $x = 1/8$ compound, a phase transition from the FM metallic phase to the FM insulating phase occurs at 150 K.[10] Recently, a neutron diffraction study revealed that a FM moment of 3.43 μ_B/Mn is directed mainly along the b axis in the monoclinic $P12_1/c1$ structure at 5 K, and that the FM spin orientation changes from the b axis to the c axis in the b-c plane with increasing temperature as shown in Fig. 1(b).[17]

A polycrystalline bulk sample of LSMO ($x = 1/8$) was synthesized by a conventional solid-state reaction. The starting materials, La$_2$O$_3$, SrCO$_3$, and Mn$_3$O$_4$, were mixed with the nominal ratio and calcined in air at 1000 °C and 1350 °C with intermediate grinding. A thin-plate specimen was obtained by mechanical grinding and Ar^+ ion sputtering with an accelerating voltage of 3.5 kV at a low temperature using liquid nitrogen for the sintered pellet. The sample was observed using a FEI Titan Cubed transmission electron microscope (TEM) equipped with a liquid-nitrogen-type cooling holder. The *in situ* LM observation was conducted at 300 kV using an objective lens to apply magnetic fields and a Lorentz lens located immediately below the objective lens; magnetic fields of −2.8 kOe (downward)—3.6 kOe (upward) were applied along the direction normal to the sample plane while controlling the excitation of the objective lens. An additional lens located below the Lorentz lens was used for defocusing the image. The sample thickness was measured by electron energy-loss spectroscopy (EELS)[18] combined with scanning TEM (STEM) at 80 kV. The in-plane magnetization was analyzed by a phase retrieval technique based on the transport of intensity equation (TIE).[19,20] The magnetization

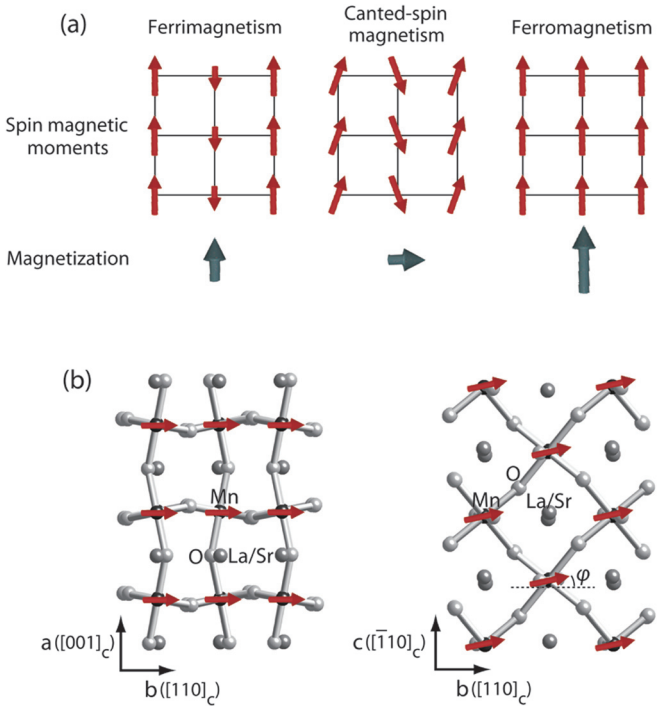

FIG. 1. (a) Schematic of spin arrangements in magnetic phases exhibiting spontaneous magnetization: ferrimagnetism, canted-spin magnetism, and ferromagnetism. (b) Basic crystal structure with monoclinic $P12_1/c1$ symmetry and FM spin orientation of lightly doped perovskite manganite LSMO at $x = 1/8$ below 187 K revealed by Li *et al.* by neutron diffraction analysis.[17] The directions in parentheses are described in a pseudocubic perovskite setting. The spin orientation changes from the *b* axis to the *c* axis in the *b*-*c* plane with increasing temperature; the estimated values of φ are ~0.3° at 5 K, ~12.0° at 100 K, and ~59.7° at 170 K.

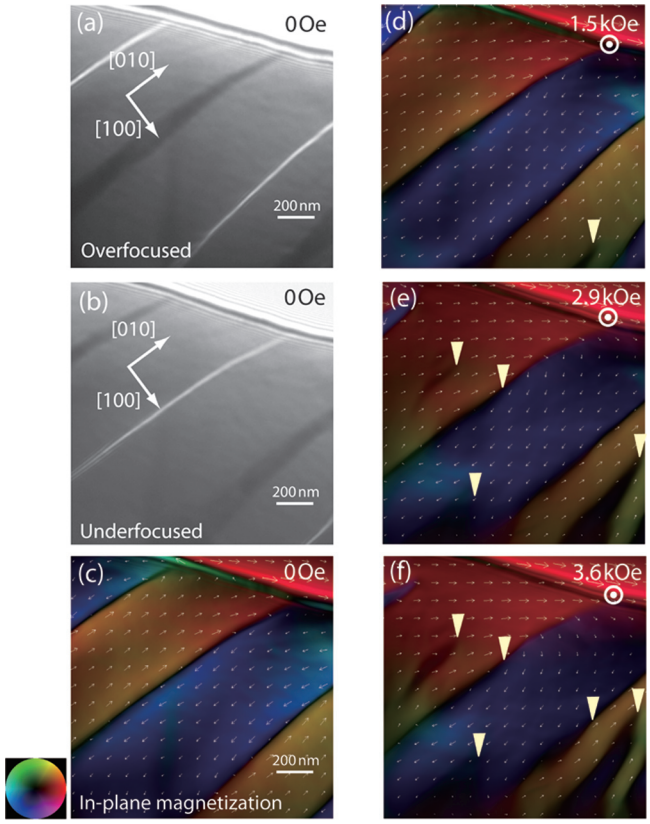

FIG. 2. Variation in in-plane magnetization in the 180° domain structure of the FM LSMO at 100 K with external magnetic field normal to the sample plane. (a) Overfocused Lorentz image with $\Delta f = -300$ μm at 0 Oe. (b) Underfocused Lorentz image with $\Delta f = 300$ μm at 0 Oe. (c) In-plane magnetization at 0 Oe analyzed by the TIE method using the images in (a) and (b). The colors and arrows represent the direction and magnitude of magnetization (see the color wheel). (d)–(f) In-plane magnetization at (d) 1.5 kOe, (e) 2.9 kOe, and (f) 3.6 kOe obtained by analysis. The magnitude is reduced in the additional domains shown by triangles. The magnetization in these domains has large perpendicular components.

distribution was calculated from the electron phases, which were retrieved using the intensity of three Lorentz images with defocus values (Δf) of ± 300 μm and 0 μm.

First, we observed the magnetic domain structure under no magnetic field. During zero-field cooling, magnetic contrast appeared in the Lorentz images below ~180 K. Figures 2(a) and 2(b), respectively, show the overfocused and underfocused Fresnel images ($\Delta f = \pm 300$ μm) observed along the [001] direction at 100 K in the FM insulating phase. The alternating sharp bright and broad dark lines in each image correspond to the magnetic domain walls in the sample. Interference fringes called Fresnel fringes are observed at the edge of each specimen because the mean inner potential of the material gives a phase difference between the electron wave in the specimen and in the vacuum. The in-plane magnetization obtained by analysis of these images using the TIE method is shown in Fig. 2(c), where the colors and arrows represent the direction and magnitude of magnetization. These indicators clearly show a 180° domain structure, where the magnetization is antiparallel between neighboring domains, whereas artifacts appear near the edge of the specimen owing to the Fresnel fringes. The domain walls are almost along the [010] direction, which is close to the direction of the axis of easy magnetization.[17]

Next, we applied perpendicular magnetic fields to the same area of the specimen. The direction of the fields was along the [001] direction of the crystal and roughly normal to the axis of easy magnetization. Figure 2(d) shows the in-plane magnetization at 1.5 kOe obtained by analysis. Whereas the application of fields of up to 1.5 kOe did not induce striking changes in the magnetization, the formation of an anisotropic domain with a reduced in-plane component (indicated by a triangle) was observed at a magnetic field of 1.5 kOe. Because the decrease in the in-plane component is attributed to the increase in the perpendicular component, the magnetization in the additional domain should have a large perpendicular component. The number and size of domains having a large perpendicular component increase with increasing intensity of the field as shown in Figs. 2(e) and 2(f).

When the axis of easy magnetization is at a large angle to the sample plane, the response of the spin arrangement to the external magnetic field is markedly different. Figure 3(a) shows the in-plane magnetization analyzed using Lorentz images observed along the [011] direction at 100 K in the FM insulating phase. Serpentine-like domains, which exhibit magnetization along the axis of easy magnetization,[21] are formed at 0 Oe since the axis is close to the normal to the surface (middle panel). The deviation of the axis from the normal direction results in in-plane components of magnetization along the $[01\bar{1}]$ or $[0\bar{1}1]$ direction. It is estimated from the tilting of the easy axis that the perpendicular component is along the [011] (downward into the plane) and $[0\bar{1}\bar{1}]$ (upward) directions in domains having the in-plane

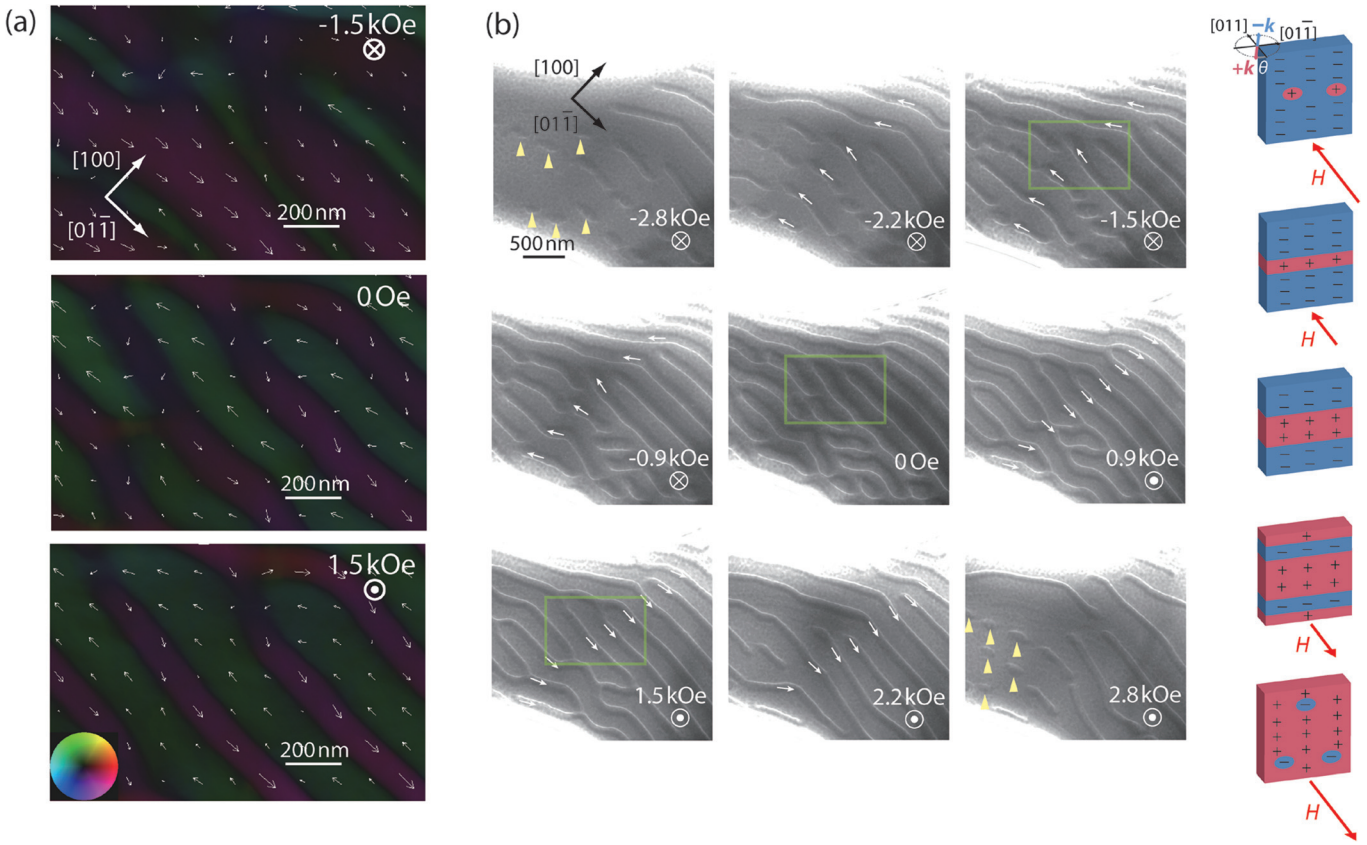

FIG. 3. (a) Variation in in-plane magnetization in the serpentine-like domain structure at 100 K with the perpendicular magnetic field (−1.5 kOe, 0 Oe, and 1.5 kOe). (b) Lorentz images with $\Delta f = -300$ μm at 100 K for magnetic fields of −2.8–2.8 kOe, where the green rectangles show the area analyzed in (a). The domains indicated by arrows are deteriorated by the fields, resulting in nanoscale elliptical magnetic bubbles shown by triangles. The inset shows a schematic of the formation of magnetic bubbles, where the signs "+" and "−" denote that the magnetization is along the $+\boldsymbol{k}$ and $-\boldsymbol{k}$ directions, respectively, and the angle θ is estimated to be approximately 33°.

component along the [01$\bar{1}$] and [0$\bar{1}$1] directions, respectively. The widths of domains having opposite directions of magnetization are almost the same at 0 Oe. The application of a perpendicular field causes a continuous change in the domain structure. The width of domains having the in-plane component along the [01$\bar{1}$] direction gradually increases with increasing magnetic field from 0 to −1.5 kOe. In contrast, it gradually decreases with increasing magnetic field from 0 to 1.5 kOe. In both cases, the magnetic field causes the growth of domains having a perpendicular component parallel to the field and the deterioration of domains having a component antiparallel to the field.

Here, we found that stronger fields lead to the formation of magnetic bubbles, as shown in Fig. 3(b). The width of the domains indicated by arrows decreases with increasing magnetic field. Stronger fields divided the domains into pieces, which were further reduced in size and transformed into small bubble domains indicated by triangles. These domains have an elliptical shape elongated along the [01$\bar{1}$] direction, which is attributed to the tilting of the easy axis because the projection of the axis on the plane corresponds to the major axis. The anisotropy of the domain-wall energy density in the plane results from the deviation of the easy axis from the normal direction, causing the elliptical bubble domains.[22] We show a schematic of their formation in the inset. We also observed the extinction of magnetic bubbles by magnetic fields as shown in Fig. 4(a). Some of the bubbles that existed at 3.4 kOe (indicated by arrows) disappeared at 3.6 kOe. A theoretical study on the stability of magnetic bubbles has shown that the intensity of the external field in which stable bubbles can exist increases with increasing thickness of the sample.[23] The sample prepared by ion milling was wedge-shaped, as shown by the thickness profile, and hence only the bubbles near the edge vanished.

A striking feature of the magnetic bubbles in the FM insulating phase of LSMO is their small size; the bubbles had a ~100 nm minor diameter and ~200 nm major diameter at 3.6 kOe. It has been reported that the diameter of magnetic bubbles (d) is proportional to $K_u^{1/2} I_s^{-2}$.[2] The saturation magnetization of LSMO at 100 K when $x = 1/8$ has a very large value of $I_s = 7.3 \times 10^{-1}$ Wbm^{-2} compared with that of other bubble materials such as ferrimagnetic iron-garnets $R_3(Fe,M)_5O_{12}$ and spin-canted orthoferrites $RFeO_3$.[17] Figure 4(b) shows the values of I_s^{-2} and d for the FM LSMO and other bubble materials.[3,4] Here, the formation of the bubbles directly shows that the material has large magnetic anisotropy because the necessary condition for bubble formation is $K_u \geq I_s^2/2\mu_0$;[23] the anisotropy of the FM insulating phase at 100 K is more than 2.1×10^5 J/m^3. The large anisotropy is considered to originate from the ordering of the Mn 3d (e_g) orbital in the FM insulating phase ($T_{oo} = 150$ K). It has been reported that magnetic anisotropy can be enhanced by the strain in epitaxial LSMO films,[24–27] however, we can clearly reject the possibility that the present sample was subjected to a significant amount of lattice strain due to the sample preparation, because no bend contours, a type of diffraction

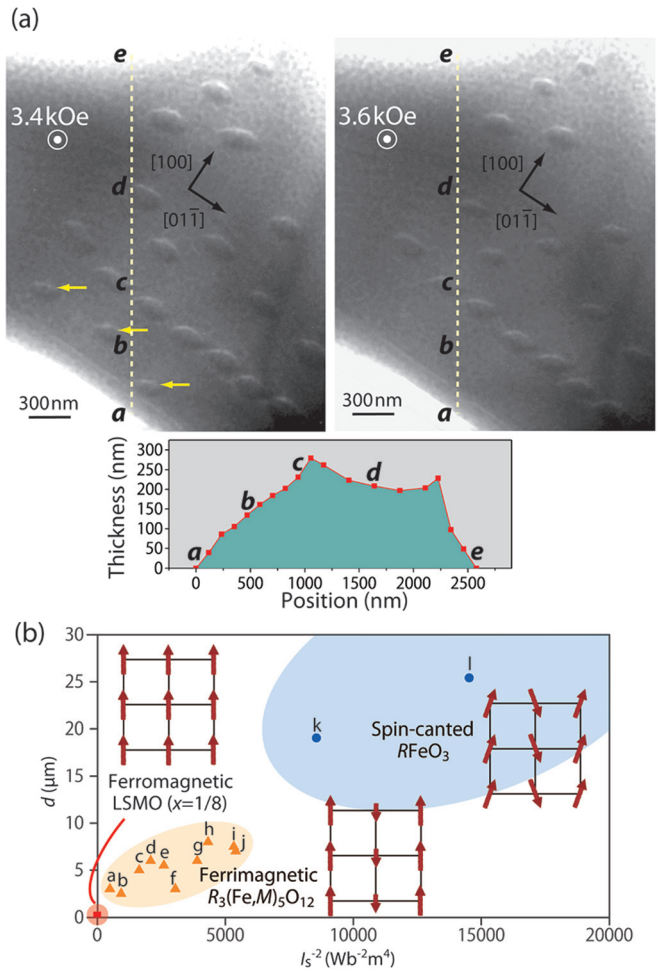

FIG. 4. (a) Lorentz images with $\Delta f = -300$ μm at 100 K showing extinction of magnetic bubbles at 3.6 kOe and the sample thickness profile measured by EELS. The letters *a*-*e* represent some of the positions where the thickness was measured. (b) Values of I_s^{-2} (I_s: saturation magnetization) and d (diameter of magnetic bubbles) of the FM insulating phase of LSMO and other bubble materials: ferrimagnetic iron-garnets $R_3(Fe,M)_5O_{12}$ and spin-canted orthoferrites $RFeO_3$ (a: $Y_{1.8}Eu_{0.2}Gd_{0.5}Tb_{0.5}Al_{0.6}Fe_{4.4}O_{12}$, b: $Y_2GdAl_{0.8}Fe_{4.2}O_{12}$, c: $EuEr_2Ga_{0.7}Fe_{4.3}O_{12}$, d: $Eu_{1.5}Gd_{1.5}Al_{0.5}Fe_{4.5}O_{12}$, e: $Eu_2ErGa_{0.7}Fe_{4.3}O_{12}$, f: $Gd_{0.95}Tb_{0.75}Er_{1.3}Al_{0.5}Fe_{4.5}O_{12}$, g: $Eu_{1.9}Gd_{1.1}Al_{0.5}Fe_{4.5}O_{12}$, h: $PrGd_2Ga_{0.5}Fe_{4.5}O_{12}$, i: $Gd_{2.34}Tb_{0.66}Fe_5O_{12}$, j: $Er_2TbAl_{1.1}Fe_{3.9}O_{12}$, k: $Sm_{0.55}Tb_{0.45}FeO_3$, l: $Sm_{0.6}Er_{0.4}FeO_3$).[3,4]

contrast which would have indicated strain in the crystal, were observed in the conventional TEM image.

The crystalline magnetic anisotropy is quite small in the FM metallic phases of LSMO single crystals,[8,28,29] in which the orbital is disordered. On the other hand, long-range ordering of the orbital has been directly observed by Geck *et al.* for the FM insulating phase of an $x = 1/8$ single crystal using resonant x-ray scattering.[14] The ordering temperature increases with increasing doping level x in the range $0.11 \leq x \leq 0.15$ from ~120 to ~180 K.[10–12] Woods *et al.* reported the results of a reversible transverse susceptibility experiment for an $x = 0.15$ single crystal, which indicated a rapid increase in the anisotropy field around T_{oo} (~180 K) with decreasing temperature.[30] The data reported by Urushibara *et al.* show that the saturation magnetization at 100 K in the OO FM insulating state is almost equal to that at 200 K in the orbital-disordered FM metallic state, I_s (100 K)/I_s (200 K) = 1.2;[8] we calculated that the effective anisotropy constant at 100 K is 3.7 times larger than that at 200 K using the data reported by Woods *et al.* The orbital ordering shows clear anisotropy in the monoclinic $P12_1/c1$ structure; hole-poor and hole-rich planes alternate along the a axis, which is perpendicular to the axis of easy magnetization. We therefore deduced that the orbital ordering enhances the magnetic anisotropy through the strong coupling of the spin, orbital, and lattice. Orbital-order-induced strong magnetic anisotropy has also been observed for the FM phases of other materials including (Pr, Sr)MnO_3 single crystals.[31]

While FM crystals are materials potentially giving rise to very small bubbles owing to the large I_s in accordance with the relation $d \propto K_u^{1/2} I_s^{-2}$, most of them do not satisfy the condition $K_u \geq I_s^2/2\mu_0$ because the required value of K_u is too large owing to the large I_s. However, our study revealed that the value of K_u for the OO FM insulating phase is sufficiently large to realize nanoscale magnetic bubbles. This finding provides a route for realizing nanoscale bubbles using FM phases with the anisotropy enhanced by orbital ordering. The very small bubble size is highly desirable for the achievement of ultrahigh recording density. Moreover, these results suggest the possibility of manipulating the bubbles using an electric field because the present LSMO phase is a multiorbital Mott insulator. A generic mechanism exists for the coupling of the external electric field $\mathbf{E}$ to the internal electric field $\mathbf{e}$ originating from the dynamical spin Berry phase in multiorbital Mott insulators.[5,6] Magnetic defects such as magnetic bubbles, Skyrmions, and magnetic vortices carry a nonzero topological charge (Q).[32] Mostovoy *et al.* theoretically predicted the rotational motion of the center-of-mass coordinates (R_x, R_y) of defects induced by a rotating electric field, $\mathbf{E}(t) = E_\omega$ (cosΩt, -sgn(Q)sinΩt), where $\Omega = A/(4\pi|Q|)$, in a disk of a material with a confining potential of $U = A(R_x^2 + R_y^2)/2$.[5] Therefore, we provide the experimental results showing that magnetic bubbles can form in a FM multiorbital Mott insulator and suggesting the possibility of manipulating bubbles forming in such an insulator using an electric field.

In summary, we have directly observed nanoscale magnetic bubbles in a multiorbital Mott insulator, the OO FM insulating phase of $La_{7/8}Sr_{1/8}MnO_3$, by low-temperature *in situ* LM. Whereas magnetic fields normal to the sample plane induced anisotropic-shaped domains having large perpendicular components of magnetization in the 180° domain structure, they induced continuous changes in the width of domains in the serpentine-like domain structure. In the latter case, fields of more than ~2.8 kOe gave rise to nanoscale elliptical magnetic bubbles; the bubbles were ~100 nm in minor diameter and ~200 nm in major diameter at 3.6 kOe. The small size of the bubbles is attributed to the large saturation magnetization inherent in the FM state. We deduced that orbital ordering causes the large magnetic anisotropy through the strong coupling of the spin, orbital, and lattice, resulting in the formation of nanoscale magnetic bubbles. These results are expected to lead to the manipulation of nanoscale bubbles in multiorbital Mott insulators using an electric field.

We are grateful to A. Béché (FEI France) and C. Arm (CEA-INAC) for the calibration data of the magnetic field of the objective lens. This work was supported by a Grant-in-Aid for Young Scientists from JSPS (No. 23710115).

[1]M. Bibes and A. Barthélémy, Nature Mater. **7**, 425 (2008).
[2]A. H. Bobeck, Bell Syst. Tech. J. **46**, 1901 (1967).
[3]A. H. Bobeck, R. F. Fischer, A. J. Perneski, J. P. Remeika, and L. G. Van Uitert, IEEE Trans. Magn. **MAG-5**, 544 (1969).
[4]A. H. Bobeck, D. H. Smith, E. G. Spencer, L. G. Van Uitert, and E. M. Walters, IEEE Trans. Magn. **MAG-7**, 461 (1971).
[5]M. Mostovoy, K. Nomura, and N. Nagaosa, Phys. Rev. Lett. **106**, 047204 (2011).
[6]N. Nagaosa and Y. Tokura, Phys. Scr. **T146**, 014020 (2012).
[7]Y. Murakami, J. P. Hill, D. Gibbs, M. Blume, I. Koyama, M. Tanaka, H. Kawata, T. Arima, Y. Tokura, K. Hirota, and Y. Endoh, Phys. Rev. Lett. **81**, 582 (1998).
[8]A. Urushibara, Y. Moritomo, T. Arima, A. Asamitsu, G. Kido, and Y. Tokura, Phys. Rev. B **51**, 14103 (1995).
[9]Y. Yamada, O. Hino, S. Nohdo, R. Kanao, T. Inami, and S. Katano, Phys. Rev. Lett. **77**, 904 (1996).
[10]T. Niemöller, M. von Zimmermann, S. Uhlenbruck, O. Friedt, B. Büchner, T. Frello, N. H. Andersen, P. Berthet, L. Pinsard, A. M. De Lëon-Guevara, A. Revcolevschi, and J. R. Schneider, Eur. Phys. J. B **8**, 5 (1999).
[11]G.-L. Liu, J.-S. Zhou, and J. B. Goodenough, Phys. Rev. B **64**, 144414 (2001).
[12]G. Papavassiliou, M. Pissas, G. Diamantopoulos, M. Belesi, M. Fardis, D. Stamopoulos, A. G. Kontos, M. Hennion, J. Dolinsek, J.-Ph. Ansermet, and C. Dimitropoulos, Phys. Rev. Lett. **96**, 097201 (2006).
[13]T. Asaka, S. Mori, Y. Horibe, K. Takenaka, X. Z. Yu, T. Nagai, K. Kimoto, T. Hirayama, and Y. Matsui, Phys. Rev. B **83**, 174401 (2011).
[14]J. Geck, P. Wochner, S. Kiele, R. Klingeler, P. Reutler, A. Revcolevschi, and B. Büchner, Phys. Rev. Lett. **95**, 236401 (2005).
[15]R. I. Dass, J.-Q. Yan, and J. B. Goodenough, Phys. Rev. B **68**, 064415 (2003).
[16]S. Mori, T. Asaka, Y. Horibe, Y. Matsui, and K. Takenaka, J. Electron. Microsc. **54**(Suppl. 1), i65 (2005).
[17]H.-F. Li, Y. Su, Y. G. Xiao, J. Persson, P. Meuffels, and Th. Brückel, Eur. Phys. J. B **67**, 149 (2009).
[18]R. F. Egerton, *Electron Energy-Loss Spectroscopy in the Electron Microscope* (Plenum, New York, 1996), pp. 301–312.
[19]K. A. Nugent, T. E. Gureyev, D. F. Cookson, D. Paganin, and Z. Barnea, Phys. Rev. Lett. **77**, 2961 (1996).
[20]M. Beleggia and Y. Zhu, *Modern Techniques for Characterizing Magnetic Materials*, edited by Y. Zhu (Kluwer Academic, London, 2005), Chap. 7.
[21]E. Tatsumoto and K. Hara, Jpn. J. Appl. Phys. Part 1 **7**, 176 (1968).
[22]M. A. Popov and I. V. Zavislyak, Phys. Solid State **51**, 87 (2009).
[23]A. A. Thiele, J. Appl. Phys. **41**, 1139 (1970).
[24]C. Kwon, M. C. Robson, K.-C. Kim, J. Y. Gu, S. E. Lofland, S. M. Bhagat, Z. Trajanovic, M. Rajeswari, T. Venkatesan, A. R. Kratz, R. D. Gomez, and R. Ramesh, J. Magn. Magn. Mater. **172**, 229 (1997).
[25]Y. Wu, Y. Suzuki, U. Rüdiger, J. Yu, A. D. Kent, T. K. Nath, and C. B. Eom, Appl. Phys. Lett. **75**, 2295 (1999).
[26]J. Dho, Y. N. Kim, Y. S. Hwang, J. C. Kim, and N. H. Hur, Appl. Phys. Lett. **82**, 1434 (2003).
[27]S. R. Bakaul, W. Lin, and T. Wu, Appl. Phys. Lett. **99**, 042503 (2011).
[28]J. Zabaleta, M. Jaafar, P. Abellán, C. Montón, O. Iglesias-Freire, F. Sandiumenge, C. A. Ramos, R. D. Zysler, T. Puig, A. Asenjo, N. Mestres, and X. Obradors, J. Appl. Phys. **111**, 024307 (2012).
[29]N. A. Viglin, S. V. Naumov, and Ya. M. Mukovskiĭ, Phys. Solid State **43**, 1934 (2001).
[30]G. T. Woods, P. Poddar, H. Srikanth, and Ya. M. Mukovskii, J. Appl. Phys. **97**, 10C104 (2005).
[31]S. Cao, B. Kang, J. Zhang, and S. Yuan, Appl. Phys. Lett. **88**, 172503 (2006).
[32]A. A. Belavin and A. M. Polyakov, JETP Lett. **22**, 245 (1975).